Chapter 12

On a New Numerical Approach on Micropolar Fluid, Heat and Mass Transfer Over an Unsteady Stretching Sheet Through Porous Media in the Presence of a Heat Source/Sink and Chemical Reaction

Stanford Shateyi, Fazle Mabood and
Gerald Tendayi Marewo

Additional information is available at the end of the chapter

http://dx.doi.org/10.5772/63800

Abstract

The problem of MHD micropolar fluid, heat and mass transfer over unsteady stretching sheet through porous medium in the presence of a heat source/sink and chemical reaction is presented in this chapter. By applying suitable similarity transformations, we transform the governing partial differential equations into a system of ordinary differential equations. We then apply the recently developed numerical technique known as the Spectral Quasi-Linearization Method. The validity of the accuracy of the technique is checked against the bvp4c routine method. Numerical results for the surface shear stresses, Nusselt number and the Sherwood number are presented in tabular form. Also numerical results for the velocity, temperature and concentration distribution are presented in graphical forms, illustrating the effects of varying values of different parameters.

Keywords: micropolar fluid, unsteady stretching sheet, porous media, heat source/sink, Spectral Quasi-Linearization Method

1. Introduction

The boundary layer flows, heat and mass transfer in a quiescent Newtonian and non-Newtonian fluid driven by a continuous stretching sheet are of significance in a number of industrial engineering processes such as the drawing of a polymer sheet or filaments extruded continu-

ously from a die, the cooling of a metallic plate in a bath, the aerodynamic extrusion of plastic sheets, the continuous casting, rolling, annealing and thinning of copper wires, the wires and fibre coating. During its manufacturing process, a stretched sheet interacts with ambient fluid thermally and mechanically. Both the kinematics of stretching and the simultaneous heating or cooling during such processes have a decisive influence on the quality of the final product. In [1], the effects of chemical reaction and magnetic field on viscous flow over a non-linear stretching sheet were reported. Mabood et al. [2] studied numerically MHD flow and heat transfer of nanofluid over a non-linear stretching sheet. Abel et al. [3] investigated the steady buoyancy-driven dissipative magneto-convective flow from a vertical non-linear stretching sheet. In [4], an analysis of heat transfer over an unsteady stretching sheet with variable heat flux in the presence of heat source or sink was made. Several other studies have addressed various aspects of regular/nanofluids [5–10].

Micropolar fluids are fluids with microstructure and asymmetrical stress tensor. Physically, they represent fluids consisting of randomly oriented particles suspended in a viscous medium. These types of fluids are used in analysing liquid crystals, animal blood, fluid flowing in brain, exotic lubricants, the flow of colloidal suspensions, etc. The theory of micropolar fluids was first proposed by Eringen [11]. In this theory, the local effects arising from the micro-structure and the intrinsic motion of the fluid elements are taken into account. The comprehensive literature on micropolar fluids, thermomicropolar fluids and their uses in engineering and technology was presented by Kelson and Desseaux [12]. Gorla and Nakamura [13] discussed the combined convection from a rotating cone to micropolar fluids with an arbitrary variation of surface temperature. Prathap Kumar et al. [14] studied the effect of surface conditions on the micropolar flow driven by a porous stretching sheet. In [15], the case of mixed convection flow of a micropolar fluid past a semi-infinite, steadily moving porous plate with varying suction velocity normal to the plate in the presence of thermal radiation and viscous dissipation was discussed. Mansour et al. [16] studied heat and mass transfer effects on the magnetohydrodynamic (MHD) flow of a micropolar fluid on a circular cylinder. El-Hakiem [17] proposed the dissipation effects on the MHD-free convective flow over a non-isothermal surface in a micropolar fluid. Joule heating and mass transfer effects on the MHD-free convective flow in micropolar fluid are investigated by El-Hakiem et al. [18] and El-Amin [19], respectively. In [20], the derivation of the unsteady MHD-free convection flow of micropolar fluid past a vertical moving porous plate in a porous medium was presented. Many researchers investigated different aspects of micropolar fluid [21–23].

The study of heat source/sink effects on heat transfer is another important issue in the study of several physical problems. The effect of non-uniform heat source, only confined to the case of viscous fluids, was also included in [24–27], while Mabood et al. [28] investigated non-uniform heat source/sink effects and Soret effects on MHD non-Darcian convective flow past a stretching sheet in a micropolar fluid with radiation.

Combined heat and mass transfer problems with chemical reactions are important in many processes of interest in engineering and have received significant attention in recent years. These processes include drying, evaporation at the surface of a water body, energy transfer in a wet cooling tower and the flow in a desert cooler [29]. Chemical reactions are classified as

http://dx.doi.org/10.5772/63800

either homogeneous or heterogeneous. A homogeneous reaction is one which occurs uniformly through a given phase, while a heterogeneous reaction takes place in a restricted region or within the boundary of a phase. A reaction is said to be a first-order reaction if the rate of reaction is directly proportional to the concentration [30, 31]. The effect of chemical reaction on thermal radiation for MHD micropolar flow and heat and mass transfer was investigated by Das [32]. Hayat et al. [33] considered MHD flow and mass transfer of an upper-convected Maxwell fluid past a porous shrinking sheet with chemical reaction. The behaviour of chemically reactive solute and distribution in MHD boundary layer flow over a permeable stretching sheet were investigated by Bhattacharyya and Layek [34]. Kandasamy et al. [35] studied the effect of transfer of chemically reactive species in MHD-mixed convective flow past over a porous wedge. The solution for diffusion of chemically reactive species in a flow of a non-Newtonian fluid over a stretching sheet immersed in a porous medium was reported by Afify [36], while Mabood et al. [37] reported the effects of chemical reaction and transpiration on MHD stagnation point flow and heat transfer over a stretching sheet.

The main objective of this chapter is to apply a recently developed numerical technique known as Spectral Quasi-Linearization Method (SQLM) in solving MHD micropolar fluid, heat and mass transfer over an unsteady stretching sheet through porous media in the presence of a heat source/sink and chemical reaction. The SQLM was first implemented by Motsa et al. [38].

2. Mathematical formulation

We consider an unsteady two-dimensional, mixed convection flow of a viscous incompressible micropolar fluid, heat and mass transfer over an elastic vertical permeable stretching sheet in the presence of a heat source/sink and chemical reaction. Following [39], the sheet is assumed to emerge vertically in the upward direction from a narrow slot with a velocity,

$$U_w(x,t) = \frac{ax}{1-\alpha t}, \tag{1}$$

where both a and α are positive constants with dimension per unit time. We measure the positive x direction along the stretching sheet with the top of the slot as the origin. We then measure the positive y coordinate perpendicular to the sheet and across the fluid flow. The surface temperature (T_w) and the concentration (C_w) of the stretching sheet vary along the x direction and in time t as

$$T_w(x,t) = T_\infty + \frac{bx}{(1-\alpha t)^2}, \quad C_w(x,t) = C_\infty + \frac{cx}{(1-\alpha t)^2}, \tag{2}$$

where b and c are constants with dimension temperature and concentration respectively, over length. It is noted that the expressions for $U_w(x, t)$, $T_w(x, t)$ and $C_w(x, t)$ are valid only for $t < \alpha^{-1}$. We also remark that the elastic sheet which is fixed at the origin is stretched by applying

a force in the x-direction and the effective stretching sheet rate $a/(1-\alpha t)$ increases with time. Analogously, the sheet temperature and concentration increase (reduce) if b and c are positive (negative), respectively, from T_∞ and C_∞ at the sheet in the proportion to x. We assume that the radiation effect is significant in this study. The fluid properties are taken to be constant except for density variation with temperature and concentration in the buoyancy terms. Under those assumptions and the Boussinesq approximations, the governing two-dimensional boundary layer equations are given as:

$$\frac{\partial u}{\partial x}+\frac{\partial v}{\partial y}=0, \tag{3}$$

$$\frac{\partial u}{\partial t}+u\frac{\partial u}{\partial x}+v\frac{\partial u}{\partial y}=\left(\frac{\mu+\kappa}{\rho}\right)\frac{\partial^2 u}{\partial y^2}+\frac{\kappa}{\rho}\frac{\partial N}{\partial y}+g\beta_t\left(T-T_\infty\right)+g\beta_c\left(C-C_\infty\right)-\frac{\sigma B_0^2 u}{\rho}-\frac{\nu u}{\rho K_p^*}, \tag{4}$$

$$\frac{\partial N}{\partial t}+u\frac{\partial N}{\partial x}+v\frac{\partial N}{\partial y}=\frac{\gamma}{\rho j}\frac{\partial^2 N}{\partial y^2}-\frac{\kappa}{\rho j}\left(2N+\frac{\partial u}{\partial y}\right), \tag{5}$$

$$\frac{\partial T}{\partial t}+u\frac{\partial T}{\partial x}+v\frac{\partial T}{\partial y}=\alpha_0\frac{\partial^2 T}{\partial y^2}+\left(\frac{\mu+\kappa}{\rho c_p}\right)\left(\frac{\partial u}{\partial y}\right)^2\pm\frac{Q}{\rho c_p}\left(T-T_\infty\right), \tag{6}$$

$$\frac{\partial C}{\partial t}+u\frac{\partial C}{\partial x}+v\frac{\partial C}{\partial y}=D\frac{\partial^2 C}{\partial y^2}-\kappa_c\left(C-C_\infty\right). \tag{7}$$

where u and v are the velocity components along the x and$y$ axes, respectively, T is the fluid temperature, μ is the component of the microrotation vector normal to the x y plane, γ is the spin gradient viscosity, α_0 is the thermal conductivity, C_p is the heat capacity at constant pressure, g is the acceleration due to gravity, β_t and β_c are the coefficients of thermal expression and concentration expansion, respectively, β_0 is the transverse magnetic field, C is the concentration of the solutes, T_∞ and C_∞ denote the temperature and concentration far away from the plate, respectively, and j is the microinertia density or microinertia per unit mass. The appropriate boundary conditions for the current model are:

$$u=U_w\left(x,t\right),\ v=V_w,\ N=0,\ T=T_w\left(x,t\right),\ C=C_w\left(x,t\right)\ \text{ at } y=0, \tag{8}$$

$$u=0,\ T\to T_\infty,\ C\to C_\infty\ \text{ as } y\to\infty. \tag{9}$$

http://dx.doi.org/10.5772/63800

3. Similarity analysis

In this section, we transform the partial differential equations into ordinary differential equations. Similarity techniques reduce the number of parameters, as well as improve insight into the comparative size of various terms present in the equations.

3.1. Transformation of the governing equations

In order to transform the governing Eqs. (3)–(7) into a set of ordinary differential equations, we introduce the following transformation variables [40]:

$$\eta = \sqrt{\frac{a}{\nu(1-\alpha t)}}y, \quad \psi = \sqrt{\frac{a\nu}{(1-\alpha t)}}xf(\eta), \quad N = \sqrt{\frac{a^3}{\nu(1-\alpha t)^3}}xh(\eta),$$
$$\mathrm{T} = T_\infty + \frac{bx}{(1-\alpha t)^2}\theta(\eta), \quad C = C_\infty + \frac{cx}{(1-\alpha t)^2}\phi(\eta), \tag{10}$$

where $\psi(x, y, t)$ is the physical stream function which automatically satisfies the continuity equation. Upon substituting similarity variables into Eqs. (3)–(7), we obtain the following system of ordinary equations:

$$(1+\Delta)f''' + ff'' - f'^2 - \frac{A}{2}(2f + \eta f') + \Delta h' + \lambda_1\theta + \lambda_2\phi - \left(M_1 + \frac{1}{K_p}\right)f' = 0, \tag{11}$$

$$\lambda_3 h'' + f\,h' - f'\,h - \frac{A}{2}(3h + \eta h') - \Delta B(2h + f'') = 0, \tag{12}$$

$$\frac{1}{\mathrm{Pr}}\theta'' + f\theta' - f'\theta - \frac{A}{2}(4\theta + \eta\theta') + Ec(1+\Delta)f''^2 \pm Q_x\theta + 0, \tag{13}$$

$$\frac{1}{Sc}\phi'' + f\phi' - f'\phi - K\phi - \frac{A}{2}(4\phi + \eta\phi') = 0. \tag{14}$$

Boundary conditions

The corresponding boundary conditions become:

$$f'(0) = 1, \; f(0) = f_w, \; h(0) = 0, \; \theta(0) = 1, \; \phi(0) = 1, \tag{15}$$

$$f'(\infty)=0,\ h(\infty)=0,\ \theta(\infty)=0,\ \phi(\infty)=0. \tag{16}$$

with

$$\begin{aligned}
&A=\frac{\alpha}{a},\ \Delta=\frac{\kappa}{\mu},\ \lambda_1=\frac{g\beta b}{a^2}=\frac{Gr_x}{\mathrm{Re}_x^2},\ Gr_x=\frac{g\beta(T_w-T_\infty)x^3}{\nu^2},\ \mathrm{Re}_x=\frac{U_w x}{\nu},\alpha_0=\frac{k}{\rho c_p},\\
&\lambda_2=\frac{g\beta_c}{a^2}=\frac{Gc_x}{\mathrm{Re}_x^2},\ Gc_x=\frac{g\beta_c(C_w-C_\infty)x^3}{\nu^2},\lambda_3=\frac{\gamma}{\mu j},\ B=\frac{\nu(1-\alpha t)}{ja}=\frac{\nu x}{jU_w},\ \mathrm{Pr}=\frac{\nu}{\alpha},\\
&Ec=\frac{U_w^{\,2}}{c_p(T_w-T_\infty)},M=\frac{\sigma B_0^{\,2}(1-\alpha t)}{\rho a},\ \frac{1}{K_p}=\frac{\nu(1-\alpha t)}{\rho a K_p^{\,*}},\ Q_x=\frac{Qx}{\rho c_p U_w},\ K=\frac{K_c(1-\alpha t)}{a}.
\end{aligned} \tag{17}$$

3.2. Quantities of engineering interest

The quantities of engineering interest in the present study are the skin-friction coefficient C_{fx}, the local wall couple stress M_{wx}, the local Nusselt number N_{ux} and the local Sherwood number Sh_x. The quantities are, respectively, defined by:

$$C_{fx}=\frac{2}{\rho U_w^{\,2}}\left[(\mu+\kappa)\left(\frac{\partial u}{\delta y}\right)_{y=0}+\kappa N|_{y=0}\right]=2(1+\Delta)\,\mathrm{Re}_x^{\,-1/2}\,f''(0), \tag{18}$$

$$M_{wx}=\frac{\gamma a}{\nu}\left(\frac{\partial N}{\partial y}\right)_{y=0}=\mathrm{Re}_x^{\,-1}\,h'(0), \tag{19}$$

$$Nu_x=\frac{-x}{T_w-T_\infty}\left(\frac{\partial T}{\partial y}\right)_{y=0}=-\mathrm{Re}_x^{1/2}\,\theta'(0), \tag{20}$$

$$Sh_x=\frac{-x}{C_w-C_\infty}\left(\frac{\partial C}{\partial y}\right)_{y=0}=-\mathrm{Re}_x^{1/2}\,\phi'(0). \tag{21}$$

4. Method of solution

In this section, we give a brief overview of the Spectral Quasi-linearization Method (SQLM). The SQLM uses the Newton-Raphson-based quasi-linearization method (QLM) to linearize the governing non-linear equations. The QLM was developed by [41]. The SQLM then integrates the QLM using the Chebyshev Spectral collocation method.

http://dx.doi.org/10.5772/63800

4.1. Spectral Quasi-Linearization Method (SQLM)

4.1.1. Main idea

Consider the problem of solving *n*th order non-linear differential equation

$$F\left(u,u',u'',...,u^{(n)}\right)=g\left(x\right) \text{ or } F\left(\mathbf{u}\right)=g\left(x\right), \tag{22}$$

subject to prescribed boundary conditions, where $a\le x\le b$. The SQLM consists of two basic steps: quasi-linearization and Chebyshev differentiation in that order.

Quasi-linearization: If we expand left-hand side of Eq. (22) in Taylor series about $\mathbf{v}(v, v', v'', ..., v^{(n)})=g(x)$ and re-arrange the terms in the resulting equation we get:

$$\mathbf{u}.\nabla F\left(\mathrm{v}\right)=\mathbf{v}.\nabla F\left(\mathrm{v}\right)-F\left(\mathrm{v}\right)+g\left(x\right). \tag{23}$$

If **v** is given then the previous equation can be used to solve for u. Keeping this in mind, we replace v and u with approximations $\boldsymbol{u}_r$ and $\boldsymbol{u}_{r+1}$ of **u** at the end of *r* and *r*+1 iterations, respectively. This results in the *n*th order linear differential equation

$$a_{0,r}u_{r+1}+a_{1,r}\frac{du_{r+2}}{dx}+a_{2,r}\frac{d^2u_{r+2}}{dx^2}+...+a_{\mathrm{n},r}\frac{d^nu_{r+2}}{dx^n}=R_r \tag{24}$$

Where $a_{m,r}=F_{u^{(m)}}(\mathbf{u}_r)$, $F_{u^{(m)}}=\frac{\partial F}{\partial u^{(m)}}$ and

$$R_r=a_{0,r}u_r+a_{1,r}u_r'+a_{2,r}u_r''+...+a_{\mathrm{n},r}u_r^{(m)}-F\left(\mathbf{u}_r\right)+g\left(x\right) \tag{25}$$

Chebyshev differentiation: To solve the differential Eq. (24) we start by performing the following preliminary steps.

1. Using the linear mapping

$$x\left(\xi\right)=\frac{1-\xi}{2}a+\frac{1+\xi}{2}b \tag{26}$$

we transform Eq. (24) on the physical interval [*a*, *b*], say, on the *x* axis to its equivalent

$$a_{0,r}u_{r+1} + a_{1,r}\beta\frac{du_{r+1}}{d\xi} + a_{2,r}\beta^2\frac{d^2u_{r+1}}{d\xi^2} + \ldots + a_{\mathrm{n},r}\beta^n\frac{d^nu_{r+1}}{d\xi^n} = R_r \tag{27}$$

on the computational interval [−1, 1] on the ξ axis, where $\beta = \frac{2}{b-a}$.

2. Partition interval [−1, 1] using the collocation points $\xi = \frac{\pi i}{N}$ where $i = 0, 1, 2, \ldots, N$.

Next we calculate differential Eq. (27) at each collocation point ξ_i. This is followed by approximating each derivative using the formula:

$$\frac{d^pu_r}{d\xi^p}(\xi_i) = \sum_{j=0}^{N}\left[D^p\right]_{ij}u_r(\xi_i)$$

where D is the $(N+1)\times(N+1)$ Chebyshev differentiation matrix [1]. This process is called Chebyshev differentiation. The differential Eq. (27) is then evaluated at points $\xi_0, \xi_1, \ldots..\xi_N$ with a linear system

$$A\begin{bmatrix} u_r(\xi_0) \\ u_r(\xi_1) \\ . \\ . \\ . \\ u_r(\xi_N) \end{bmatrix} = \begin{bmatrix} R_r(\xi_0) \\ R_r(\xi_1) \\ . \\ . \\ . \\ R_r(\xi_N) \end{bmatrix}$$

which upon including the boundary conditions and solving for each r generates a sequence $\{\mathbf{u}_r\}$ of approximation which we expect to converge.

4.2. Application to current problem

Eq. (14) is of the form

$$F(f, f', \phi, \phi', \phi'') = 0, \tag{28}$$

where

$$F(f, f', \phi, \phi', \phi'') = \frac{1}{Sc}\phi'' + f\phi' - f'\phi - K\phi - \frac{A}{2}(4\phi + \eta\phi'). \tag{29}$$

http://dx.doi.org/10.5772/63800

Hence quasi-linearization as directed in Section 4.2.1 replaces non-linear differential Eq. (28) with its linear counterpart

$$d_{0r}f_{r+1} + d_{1r}f'_{r+1} + d_{2r}\phi_{r+1} + d_{3r}\phi'_{r+1} + d_{4r}\phi''_{r+1} = R_r^{(3)} \tag{30}$$

where

$$d_{0r} = \phi'_r,\ d_{1r} = -\phi_r,\ \ d_{2r} = f_r' - K - 2A,\ \ d_{3r} = f_r - \frac{A}{2}\eta_r,\ d_{4r} = \frac{1}{Sc},\ R_r^{(3)} = -f_r'\phi_r + f_r\phi_r'.$$

Chebyshev differentiation replaces differential Eq. (30) with a linear system

$$A_{41} = \text{diag}\left\{\mathbf{\Phi}_r{}'\right\} - \text{diag}\left\{\mathbf{\Phi}_r\right\}\hat{D}, \tag{31}$$

$$A_{44} = \text{diag}\left\{\mathbf{F}_r{}'\right\} + \left(-K - 2A\right)I + \text{diag}\left\{\mathbf{F}_r - \frac{A}{2}\eta_r\right\}\hat{D} + \frac{1}{Sc}\hat{D}^2,$$

$$\mathrm{R}_r^{(4)} = -\mathbf{F}_r' \circ \mathbf{\Phi}_r + \mathbf{F}_r \circ \mathbf{\Phi}_r'$$

$$\mathbf{F}_{r+1} = \left[f_{r+1}(\xi_0)\, f_{r+1}(\xi_1) \ldots f_{r+1}(\xi_N)\right]^T,$$

$$\mathbf{\Phi}_{r+1} = \left[\phi_{r+1}(\xi_0)\phi_{r+1}(\xi_1) \ldots \phi_{r+1}(\xi_N)\right]^T.$$

Therefore the use of Quasi-linearization followed by Chebyshev differentiation replaces differential Eq. (14) with a linear system (31). Similarly, differential Eqs. (11)–(13) are replaced by linear systems, which if combined with a linear system (30) yield a larger linear system

$$\begin{bmatrix} A_{11} & A_{12} & A_{13} & A_{14} \\ A_{21} & A_{22} & O & O \\ A_{31} & O & A_{33} & O \\ A_{41} & O & O & A_{44} \end{bmatrix} \begin{bmatrix} \mathbf{F}_{r+1} \\ \mathbf{H}_{r+1} \\ \mathbf{\Theta}_{r+1} \\ \mathbf{\Phi}_{r+1} \end{bmatrix} = \begin{bmatrix} \mathbf{R}_r^{(1)} \\ \mathbf{R}_r^{(2)} \\ \mathbf{R}_r^{(3)} \\ \mathbf{R}_r^{(4)} \end{bmatrix} \tag{32}$$

subject to boundary conditions

$$f_{r+1}(\xi) = f_w,\ \sum_{k=0}^{N} \hat{D}_{Nk} f(\xi) = 1,\ h_{r+1}(\xi_N) = \xi_N,\ \theta_{r+1}(\xi_N) = 1,\ \phi_{r+1}(\xi_N) = 1, \tag{33}$$

$$\sum_{k=0}^{N} D_{0k} f(\xi) = 0,\ h_{r+1}(\xi_0) = 0,\ \theta_{r+1}(\xi_0) = 0,\ \phi_{r+1}(\xi_0) = 0, \tag{34}$$

where

$$A_{11} = \operatorname{diag}\left\{\mathbf{F}_r''\right\} + \left(-2\operatorname{diag}\left\{\mathbf{F}_r'\right\} - \left(A + M + \frac{1}{K_p}\right) I\right)\hat{D} + \operatorname{diag}\left\{\mathbf{F}_r - \frac{A}{2}\eta_r\right\}\hat{D}^2 + (1+\Delta)\hat{D}^3,$$

$$A_{12} = \Delta\hat{D},\ A_{13} = \lambda_1 I,\ A_{14} = \lambda_2 I,\ \mathbf{R}_r^{(1)} = \mathbf{F} \circ \mathbf{F}_r'' - \mathbf{F}_r' \circ \mathbf{F}',$$
$$\mathrm{A}_{21} = \operatorname{diag}\left\{\mathbf{H}_r'\right\} - \operatorname{diag}\left\{\mathbf{H}_r\right\}\hat{D} - \Delta B\hat{D}^2,$$

$$A_{22} = -\operatorname{diag}\left\{\mathbf{F}_r'\right\} - \left(\frac{3}{2}A + 2\Delta B\right) I + \operatorname{diag}\left\{\mathbf{F}_r - \frac{A}{2}\eta_r\right\}\hat{D} + \lambda_3\hat{D}^2,\ \ \mathbf{R}_r^{(2)} = \mathbf{F} \circ \mathbf{H}_r' - \mathbf{F}_r' \circ \mathbf{H}_r,$$
$$\mathrm{A}_{31} = \operatorname{diag}\left\{\mathbf{\Theta}_r'\right\} - \operatorname{diag}\left\{\mathbf{\Theta}_r\right\}\hat{D} + 2Ec(1+\Delta)\operatorname{diag}\left\{\mathbf{F}_r''\right\}\hat{D}^2,$$

$$\mathrm{A}_{32} = -\operatorname{diag}\left\{\mathbf{F}_r\right\} + (-2A + Q_x) I + \operatorname{diag}\left\{\mathbf{F}_r - \frac{A}{2}\eta_r\right\}\hat{D} + \frac{1}{\mathrm{Pr}}\hat{D}^2,$$
$$\mathbf{R}_r^{(3)} = Ec(1+\Delta)\mathbf{F}_r'' + \mathbf{F} \circ \mathbf{\Theta}_r' - \mathbf{F}_r' \circ \mathbf{\Theta},$$

$$\mathrm{A}_{41} = \operatorname{diag}\left\{\mathbf{\Phi}_r'\right\} - \operatorname{diag}\left\{\mathbf{\Phi}_r\right\}\hat{D},$$
$$\mathrm{A}_{42} = -\operatorname{diag}\left\{\mathbf{F}_r\right\} - (K + 2A) I + \operatorname{diag}\left\{\mathbf{F}_r - \frac{A}{2}\eta_r\right\}\hat{D} + \frac{1}{Sc}\hat{D}^2,$$
$$\mathbf{R}_r^{(4)} = -\mathbf{F}' \circ \mathbf{\Phi}_r + \mathbf{F}_r \circ \mathbf{\Phi}',$$

A o B denotes the Hadarmard product (element-wise multiplication) of matrices *A* and *B* of the same order, and *I* and *O* are the identity and zero matrices, respectively. Boundary conditions (33) and (34) of linear system (32) are in the same manner as done in [2]. This is followed by solution of linear system (32) to get approximations $f_r(\xi_c)$, $h_r(\xi_c)$, $\theta_r(\xi_c)$, $\phi_r(\xi_c)$ for each $r = 1, 2, \ldots$ and $c = 0, 1, 2, \ldots, N$. However, this last step requires suitable initial approximation for which we choose

http://dx.doi.org/10.5772/63800

$$f_0(\eta) = f_w + 1 - e^{-\eta},\ h_0(\eta) = \eta e^{-\eta},\ \theta_0(\eta) = e^{-\eta},\ \phi_0(\eta) = e^{-\eta},$$

so as to satisfy boundary conditions (33) and (34).

5. Results and discussion

The non-linear differential Eqs. (11)–(14) with boundary conditions (15)–(16) depend on several parameters, such as micropolar Δ, unsteadiness A, thermal buoyancy λ_1, solutal buoyancy λ_2, non-dimensional material λ_3, magnetic field M, local porous K_p, non-dimensional parameter B, Eckert number E_c, heat generation and/or absorption and chemical reaction. All the SQLM results presented in this work were obtained using $N = 50$ collocation points, and we are glad to highlight that convergence was achieved in just about five iterations. We take the infinity value η_∞ to be 40. Unless otherwise stated, the default values for the parameters are taken as:

Pr = 0.71, $B = 0.1$, M = 1, $Ec = 0.1$, $Sc = 0.22$, Δ Δ = 0.1, $\lambda_1 = \lambda_2 = 0.5$, $K_p = 1$, $K = 0.5$, f_w = 0.5, λ_3. In order to validate our numerical method, it was compared to MATLAB routine bvp4c which is an adaptive Lobatto quadrature iterative scheme. This is depicted in **Table 1**. In **Table 1**, we observe that the current results completely agree with the results generated by bvp4c. It is worth noting that convergence of SQLM occurs as early as at the sixth iteration and the method is extremely faster, saving *cpu* time. This gives confidence to our proposed method. We also observe in **Table 1** that the rates of transfers are greatly affected by the micropolar parameter Δ.

	$-f''(0)$		$-\theta'(0)$		$-\phi'(0)$	
Δ	bvp4c	SQLM	bvp4c	SQLM	bvp4c	SQLM
0.1	1.51831796	1.51831796	0.969700948	0.96700948	2.2273423	2.22734623
0.5	1.29335523	1.29335523	0.89967685	0.89967685	2.23825301	2.23825301
1	1.10530824	1.10530824	0.82937070	0.82937070	2.24887626	2.24887626

Table 1. Comparison of the SQLM results of f $-f''(0)$, $-\theta'(0)$, $\phi'(0)$ with those obtained by bvp4c for different values of the micropolar parameter Δ.

We observe in **Table 2** that the wall stresses, the Nusselt and Sherwood numbers are significantly affected by the changing values of the unsteadiness parameter. The skin-friction coefficient as expected increases with increasing values of the stretching parameter.

A	$-f''(0)$	$h'(0)$	$-\theta'(0)$	$-\theta'(0)$
0	1.18860026	0.03277007	0.22581676	1.34959740
1	1.51530691	0.02767645	1.21557294	1.75188835
2	1.86832868	0.02329578	2.06905446	2.36549832

Table 2. The effects of the unsteadiness parameter on $-f''(0)$, $h'(0)$, $-\theta'(0)$, $-\phi'(0)$.

Table 3 depicts the influence of the thermal buoyancy parameter on the skin friction coefficient, the local couple wall stress, the local Nusselt and Sherwood numbers. Both local wall stresses are reduced as the values of buoyancy parameters are increased but the Nusselt and Sherwood numbers increase with increasing values of the buoyancy parameters.

λ_1	$-f''(0)$	$h'(0)$	$-\theta'(0)$	$-\phi'(0)$
−0.5	1.77407269	0.03036702	1.17144784	1.73796915
0	1.64314463	0.02897505	1.19450881	1.74511388
0.5	0.46281664	0.01845219	1.34838298	1.80239822

Table 3. The influence of the thermal buoyancy parameter on the skin friction coefficient, couple stress and rate of heat and mass transfer coefficient.

K_p	$-f''(0)$	$h'(0)$	$-\theta'(0)$	$-\phi'(0)$
0.1	−0.51158820	0.01764248	1.36287821	1.81467597
5	0.33757366	0.01499546	1.39049894	1.82865098
10	0.63059835	0.01202912	1.41759309	1.84519070

Table 4. The effects of the local porous parameter on the skin friction coefficient, couple stress, rate of heat and mass transfer coefficient.

M	$-f''(0)$	$h'(0)$	$-\theta'(0)$	$-\phi'(0)$
1	1.51550691	0.02767645	1.21557294	1.75188835
3	1.91685662	0.03972746	1.16026663	1.73369138
5	2.24935200	0.03274343	1.11815954	1.72039545

Table 5. The influence of the magnetic field parameter on the skin friction coefficient, couple stress, rate of heat and mass transfer coefficient.

The effect of medium porosity on the wall stresses and the Nusselt and Sherwood numbers is depicted in **Table 4**. Porosity significantly affects the transfer rates. The effect of magnetic field parameter is depicted in **Table 5**. As expected, the presence of the magnetic field has prominent

http://dx.doi.org/10.5772/63800

effects on the skin-friction coefficient as well on the heat and mass transfer rates. The drag force that is generated by the presence of magnetic field causes significant resistance to the velocity of the fluid thus increases the wall stresses but reduces the rates of heat and mass transfer.

Table 6 shows the effects of the micropolar parameter and the non-dimensional material parameter on the wall stress. The micropolar parameter increases the values of the wall couple stress, but the non-dimensional material parameter reduces the values of the wall stress.

Δ	$h'(0)$	λ_3	$h'(0)$
0.1	0.05465849	0.1	0.22157402
0.5	0.23205149	0.2	0.08984383
1	0.39106943	0.3	0.05861008

Table 6. The effects of the micropolar parameter and the non-dimensional material parameter on the couple stress.

The influence of the micropolar parameter Δ on the axial velocity is depicted in **Figure 1**. It can be observed in **Figure 1** that axial velocity is an increasing function of the micropolar parameter. Physically, micropolar fluids show reduced drag compared to viscous fluids.

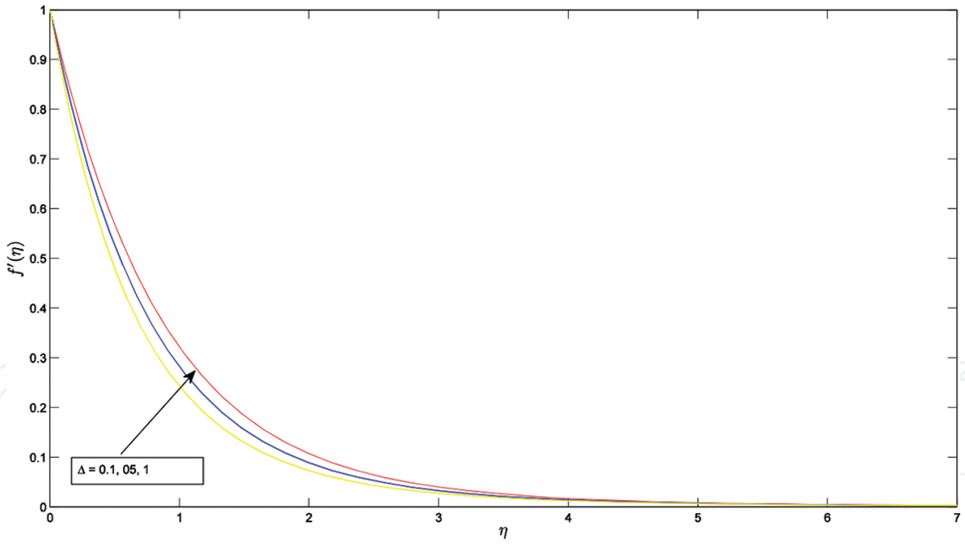

Figure 1. Velocity profile for various values of Δ.

In **Figure 2** we display the effect of unsteadiness parameter on the axial velocity $f'(\eta)$ Increasing the values of the unsteadiness parameter (A) causes the velocity boundary layer thickness to decrease, thereby reducing the velocity profiles. This is due to increased drag force on the surface. Surface stretching can therefore be used as a stabilizing mechanism in an effort to delay the transition from laminar flow to turbulent fluid flow.

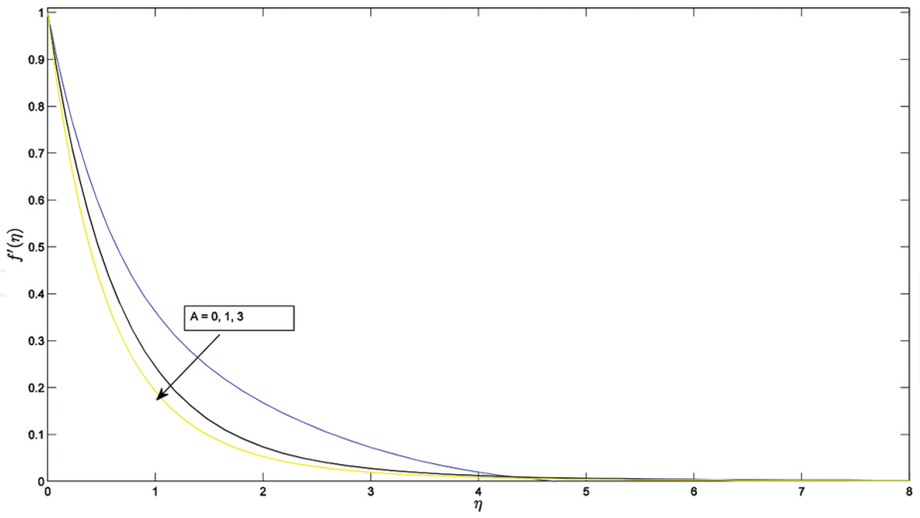

Figure 2. Velocity profile with A.

The effect of the permeability of the porous medium parameter (K_p) on the translational velocity distribution profiles is depicted in **Figure 3**. The translational velocity increases with increasing values of the porosity parameter. Physically, increasing the porosity of the medium implies that the holes of the medium become larger, thereby reducing the resistivity of the medium.

Figure 4 displays the effect of the thermal buoyancy parameter on the translational velocity distribution. The velocity profiles are reduced for the opposing flows (λ_1<0). However λ_1 becomes more positive and favourable pressure gradients are enhanced, thereby accelerating the fluid flow as can be clearly observed in **Figure 4**. It is interesting to note that for large values of the thermal buoyancy parameter, the translational velocity over-shoots near the wall over the moving speed of the sheet. This substantiates the notion that buoyancy accelerates

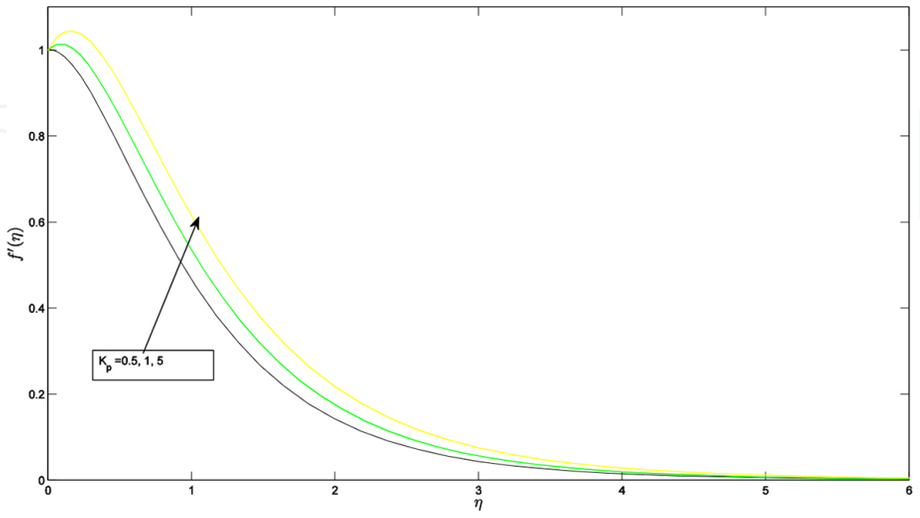

Figure 3. Variation of the porosity parameter on the axial velocity.

http://dx.doi.org/10.5772/63800

transition from laminar flow to turbulent flow; therefore, this must always be properly regulated in systems where turbulence is destructive. We also remark that solutal buoyancy as expected has the same effect as thermal buoyancy.

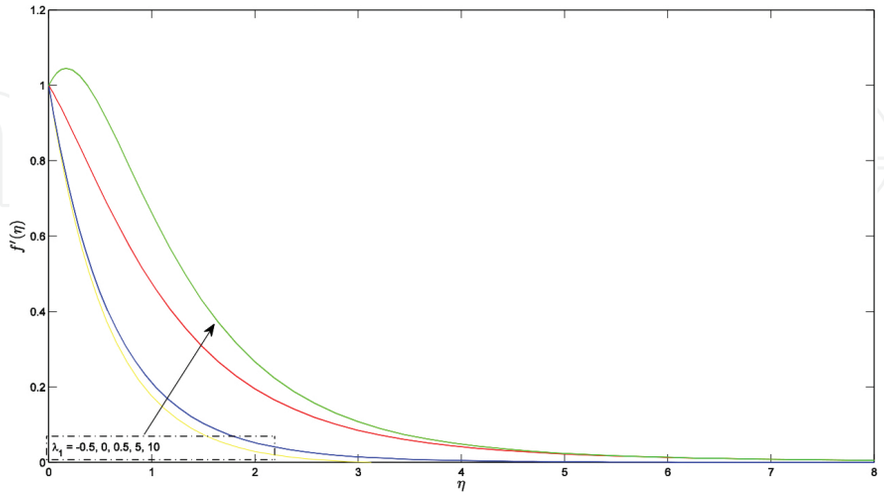

Figure 4. The influence of the thermal buoyancy on the axial velocity.

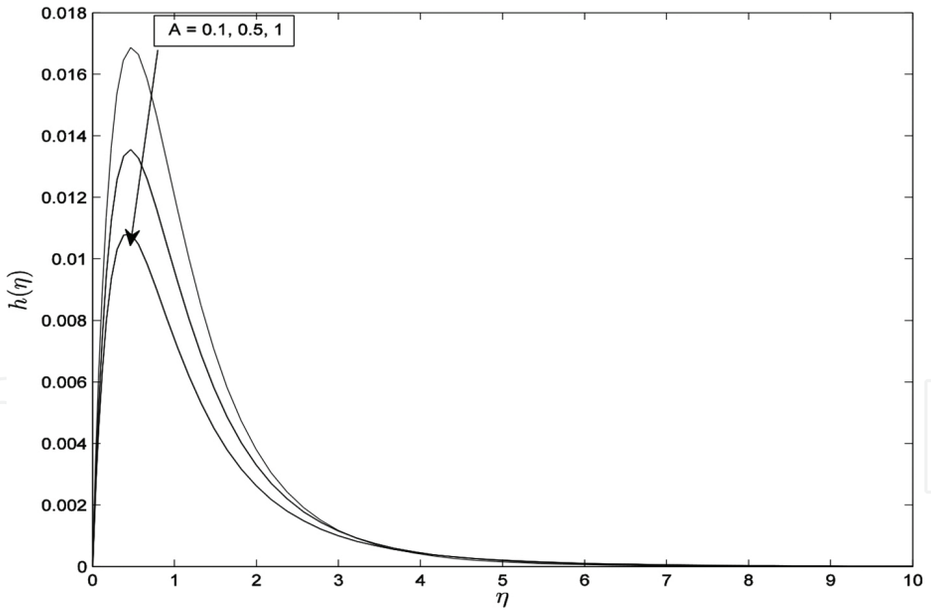

Figure 5. Variation of angular velocity with A.

The influence of the unsteadiness parameter on the angular velocity $h(\eta)$ is displayed in **Figure 5**. The unsteadiness parameter has pronounced influence on the angular velocity with values of $h(\eta)$ picking up at η=1, as can be clearly seen in **Figure 5**. However, the angular velocity approaches zero as η increases infinitely and the unsteadiness parameter (A) increases.

Figure 6 shows the effect of the microrotation parameter (B) on the angular velocity. We observe that the microrotation effect is more pronounced as expected near the surface. Increasing values of B results in much increasing values of the angular velocity profiles.

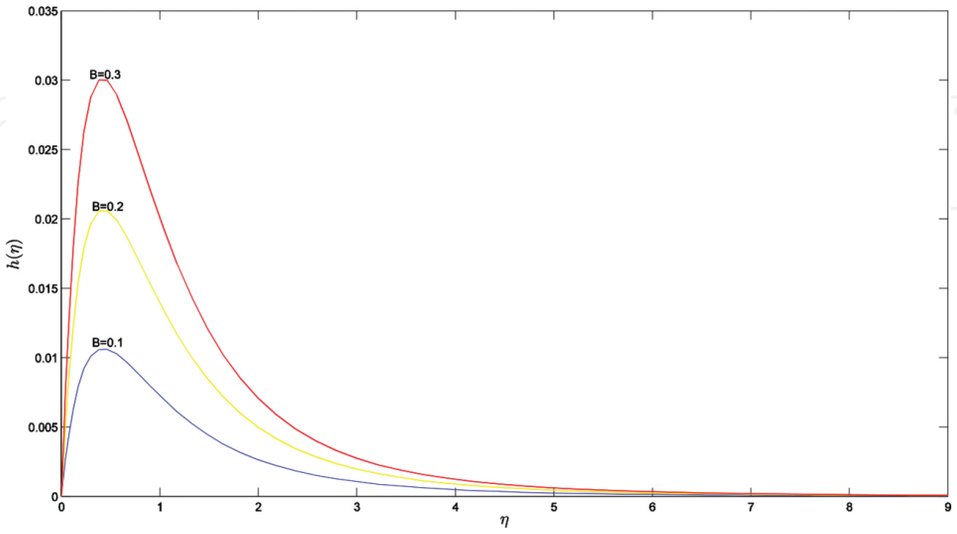

Figure 6. Influence of B on the velocity.

We observe in **Figure 7** that the angular velocity is significantly affected by the micropolar parameter (Δ) The angular velocity is greatly induced due to the vortex viscosity effect as Δ increases.

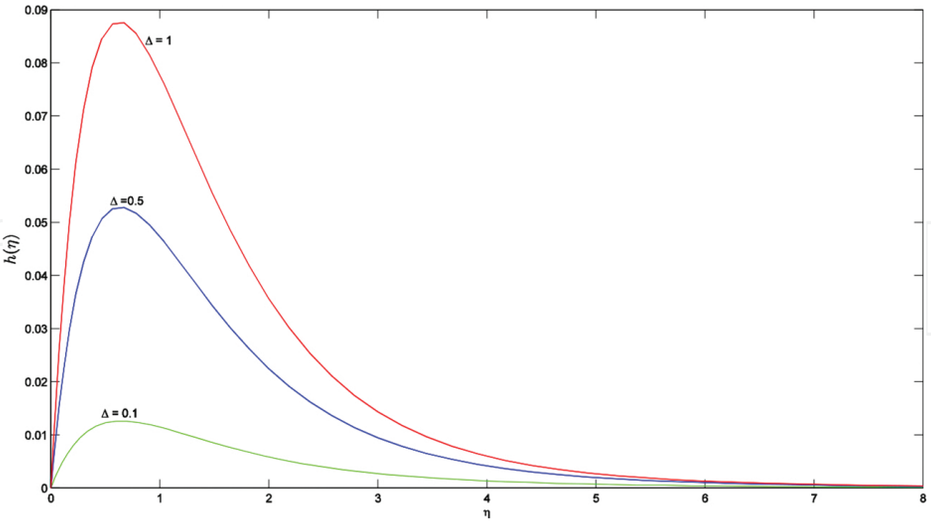

Figure 7. Variation of the angular velocity with Δ.

The effect of thermal buoyancy parameter (λ_1) is displayed in **Figure 8**. We observe that the angular velocity $h(\eta)$ increases with increasing values of the thermal buoyancy parameter λ_1.

http://dx.doi.org/10.5772/63800

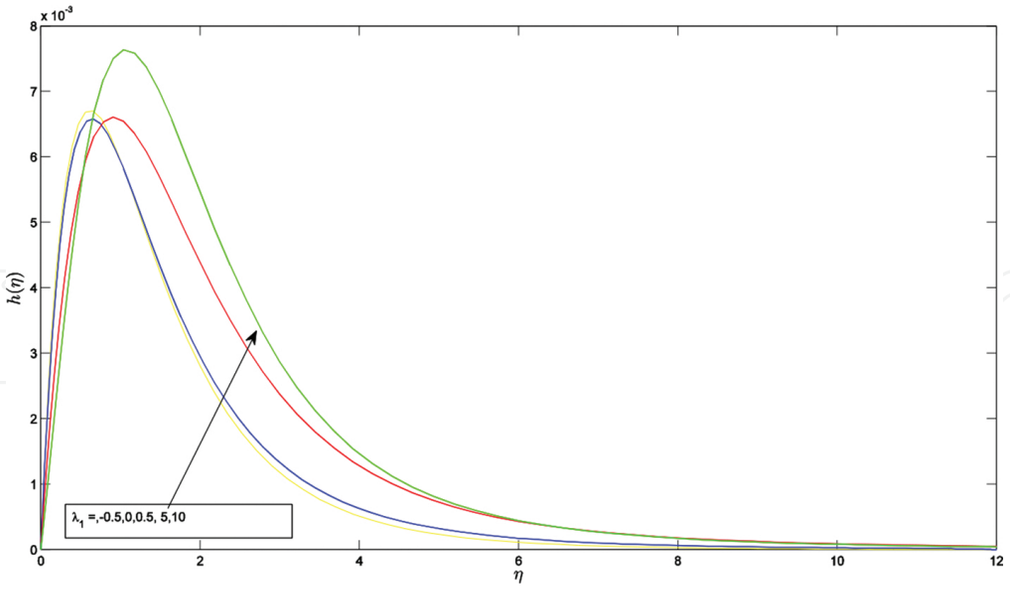

Figure 8. Angular velocity profiles for various values of thermal buoyancy.

In **Figure 9**, we display the effect of the metrical parameter on the angular velocity. The angular velocity is greatly reduced by increasing value of λ_3. This means that either the spin gradient coefficient increases or the microinertia density is reduced.

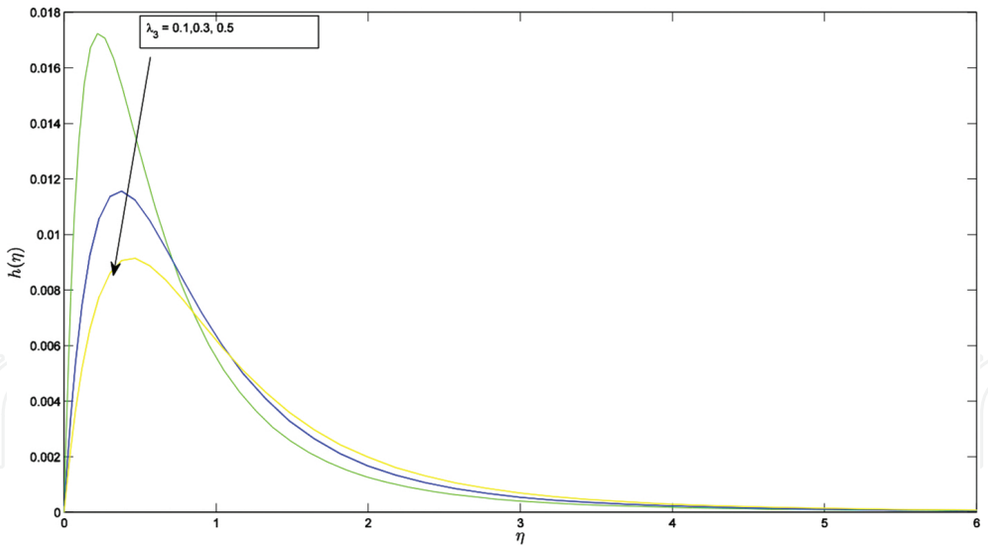

Figure 9. Variation of angular velocity with material parameter.

The effect of the unsteadiness parameter is displayed in **Figure 10**. The thermal boundary layer thickness is greatly reduced by increasing values of the unsteadiness parameter thus reducing the fluid temperature distribution

Figure 11 displays the effect of viscous dissipation on the temperature distribution resulting in increased Eckert number that causes heat energy to be stored in the region as a result of

dissipation. This dissipation is caused by viscosity and elastic deformation, thus generating heat due to the frictional heating.

The effect of thermal buoyancy parameter is depleted in **Figure 12**. The thermal boundary layer thickness is reduced when the value of the thermal buoyancy is increased. The fluid temperature is reduced at every point, except at the wall with increasing values of the thermal buoyancy parameter.

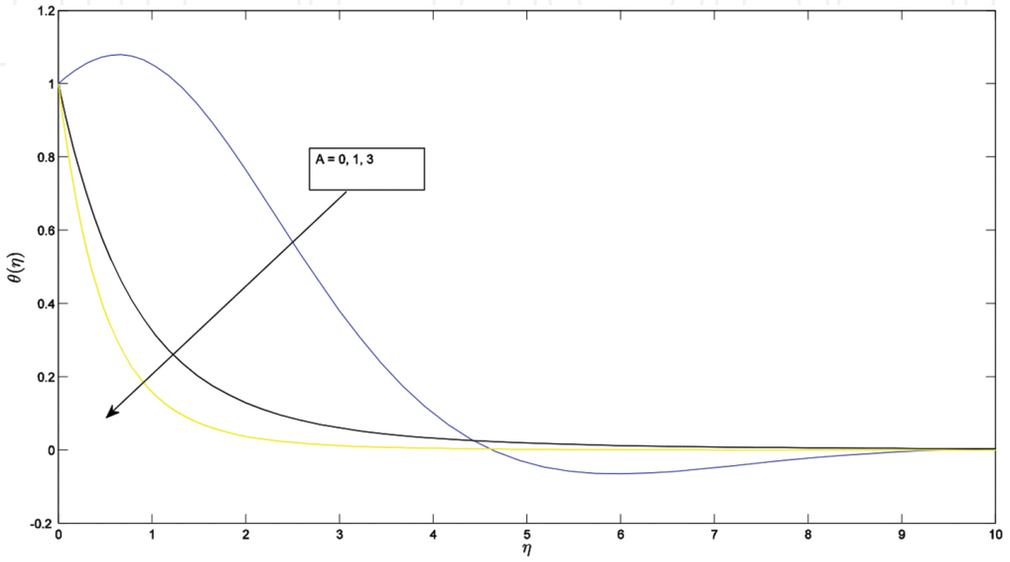

Figure 10. Temperature profile for various values of A.

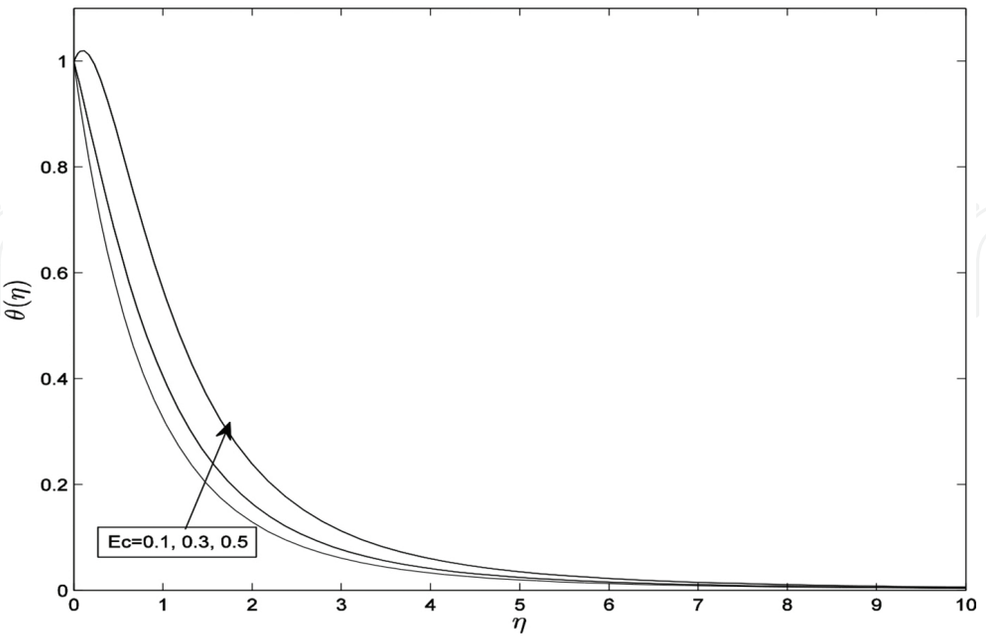

Figure 11. Variation of temperature with the Eckert number.

http://dx.doi.org/10.5772/63800

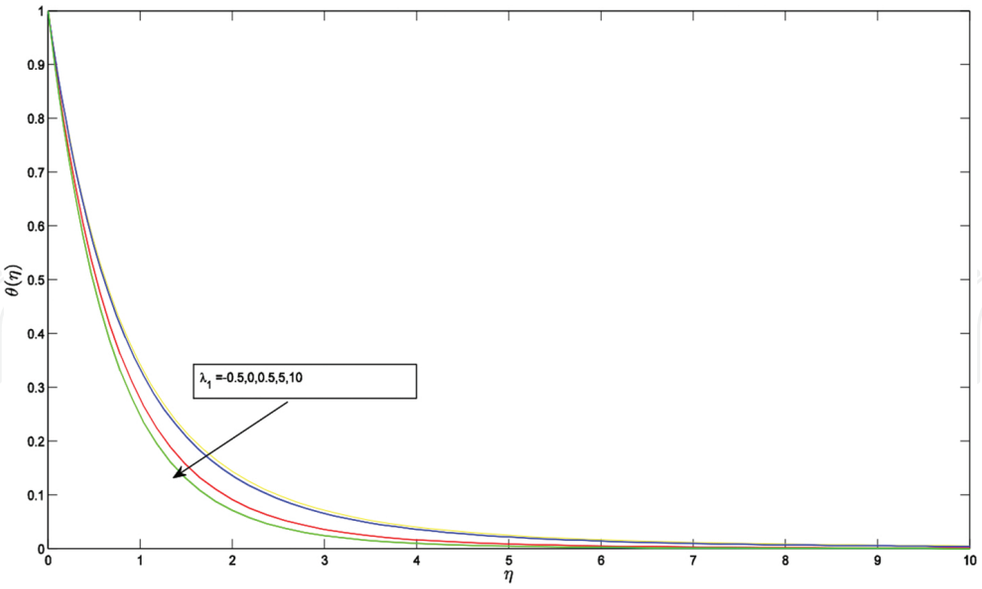

Figure 12. Temperature profile for various values of thermal buoyancy.

Figure 13 displays the variation of temperature distribution within the fluid flow for various values of the heat source/sink parameter. As expected, the fluid temperature increases with increasing values of heat at the source but decreases with increasing values of heat at a sink.

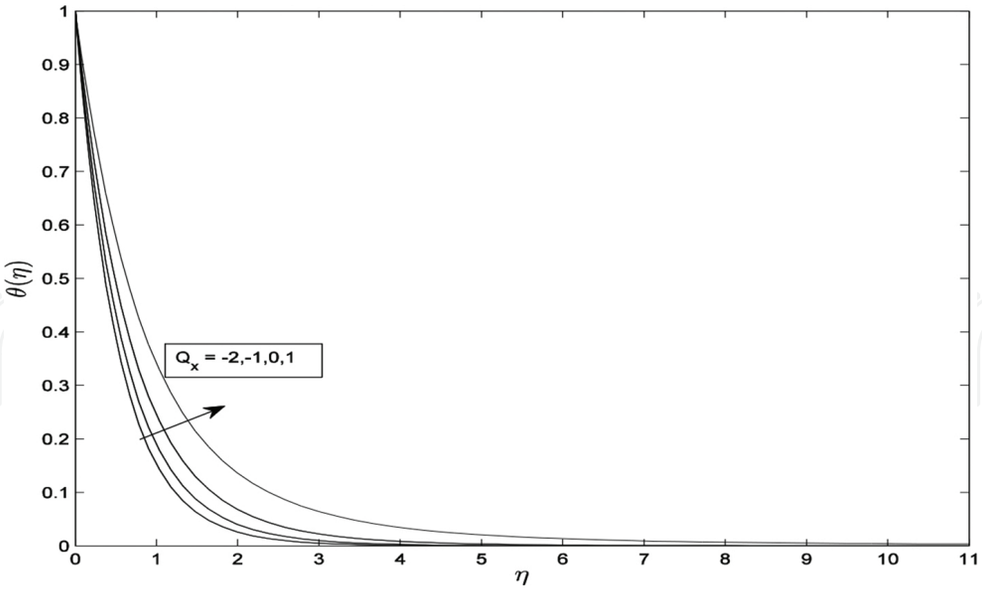

Figure 13. Temperature profile for various values of heat source/sink.

Figure 14 shows the variation of the unsteadiness parameter on the concentration profiles. It is clearly observed that increasing values of A reduces both the solutal boundary layer thickness thus reduces the concentration distributions

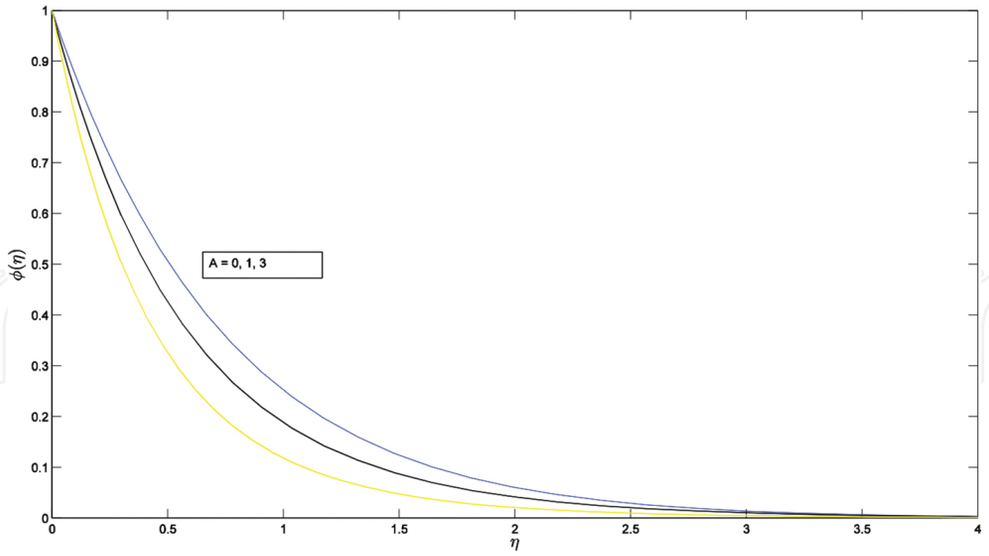

Figure 14. Concentration profile for various values A

Lastly, the influence of a chemical reaction parameter on the concentration profiles is depicted in **Figure 15**. Physically, the concentration profiles decreases as the chemical reaction parameter increases.

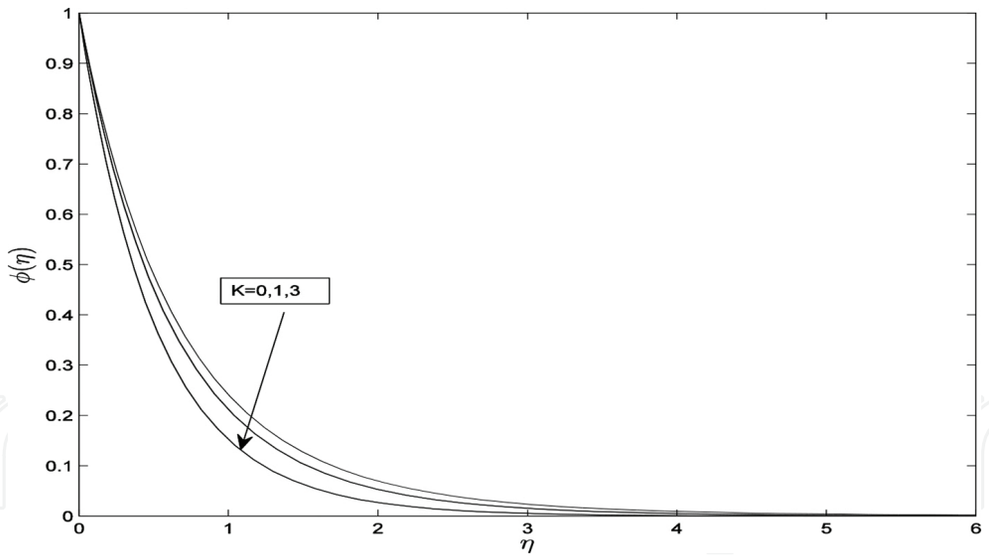

Figure 15. Variation.

6. Conclusions

The problem of MHD micropolar fluid, heat and mass transfer over unsteadiness stretching sheet through porous medium in the presence of a heat source/sink and chemical reaction is

studied in this chapter. By applying suitable similarity transformations, we transformed the governing partial differential equations into a system of ordinary differential equations. We then applied the recently developed numerical technique known as the SQLM to solve the resultant set of non-linear ordinary differential equations. The accuracy of the SQLM was validated against the bvp4c routine method. We observed that the SQLM performs much better than the bvp4c in terms of rate of convergence as well cpu time.

Based on the present study, the following conclusions are made:

1. Buoyancy forces accelerate the fluid flow near the velocity boundary layer in cases of assisting flows but retard the fluid flow in cases of opposing flows.
2. The unsteadiness parameter significantly affects the fluid properties as expected.
3. Both velocity components are increasing functions of the micropolar parameter, while the temperature and concentration distributions are reduced as the micropolar parameter increases.
4. The presence of the viscous dissipation produces heat due to friction between the fluid particles which in turn causes an increase of fluid temperature.
5. The transfer rates of a micropolar fluid are greatly enhanced as either the values of the buoyancy parameter unsteadiness Prandtl or Schmidt number are increased. But these rates are reduced as either the values of the micropolar parameters, magnetic field parameter, Eckert number or chemical reaction parameter are increased.

Author details

Stanford Shateyi[1*], Fazle Mabood[2] and Gerald Tendayi Marewo[3]

*Address all correspondence to: stanford.shateyi@univen.ac.za

1 University of Venda, Department of Mathematics, Thohoyandou, South Africa

2 Department of Mathematics, University of Peshawar, Pakistan

3 University of Limpopo, Department of Mathematics & Applied Mathematics, Sovenga, South Africa

References

[1] Rapits A, Perikis C. Viscous flow over a non-linear stretching sheet in the presence of a chemical reaction and magnetic field, Int. J. Non-Linear Mech. 2006; 41: 527–529.

[2] Mabood F, Khan WA, Ismail AIM. MHD boundary layer flow and heat transfer of nanofluids over a nonlinear stretching sheet: a numerical study. J. Magn. Magn. Mater. 2015; 374: 569–576.

[3] Abel MS, Kumar KA, Ravikumara R. MHD flow and heat transfer with effects of buoyancy, viscous and joule dissipation over a nonlinear vertical stretching porous sheet with partial slip. Engineering 2011; 3: 285–291.

[4] Ebashbeshy E, Aldawody DA. Heat transfer over as unsteady stretching surface with variable heat flux in presence of heat source or sink, Comput. Math. Appl. 2010; 60: 2806–2811.

[5] Shateyi S, Prakash J. A new numerical approach for MHD laminar boundary layer flow and heat transfer of nanofluids over a moving surface in the presence of radiation, Boundary Value Probl. 2014; 2014: 2.

[6] Khan WA, Pop I. Boundary layer flow of a nanofluid past a stretching sheet, Int. J. Heat Mass Transfer 2010; 53: 2477–2483.

[7] Makinde OD, Aziz A. Boundary layer flow of a nanofluid past a stretching sheet with a convective boundary condition, Int. J. Therm. Sci. 2011; 50: 1326–1332.

[8] Mustafa M, Hayat T, Obaidat S. Boundary layer flow of a nanofluid over an exponentially stretching sheet with convective boundary conditions, Int. J. Numer. Meth. Heat Fluid Flow 2013; 23: 945–959.

[9] Rashidi MM, Ganesh NV, Abdul Hakeem AK, Ganga B. Buoyancy effect on MHD flow of nanofluid over a stretching sheet in the presence of thermal radiation, J. Mol. Liq. 2014;198: 234–238.

[10] Shateyi S. A new numerical approach to MHD flow of a Maxwell fluid past a vertical stretching sheet in the presence of thermophoresis and chemical reaction, Boundary Value Probl. 2013; 2013: 196.

[11] Eringen AC. Theory of the micropolar fluids, Math. Anal. Appl. J. 1972; 38: 481–496.

[12] Kelson NA, Desseaux A. Effect of surface condition on flow of micropolar fluid driven by a porous stretching sheet, Int. J. Eng. Sci. 2001; 39: 1881–1897.

[13] Gorla RSR, Nakamura S. Mixed convection from a rotating cone to micropolar fluids, Int. J. Heat Fluid Flow 1975; 16: 69–73.

[14] Prathap Kumar J, Umavathi JC, Chamkha AJ, Pop I. Fully developed free convective flow of micropolar and viscous fluids in a vertical channel, Appl. Math. Model. 2010; 34: 1175–1186.

[15] Ibrahim FS, Elaiw AM, Bakr AA. Influence of viscous dissipation and radiation on unsteady MHD mixed convection flow of micropolar fluids, Appl. Math. Inf. Sci. 2008; 2: 143–162.

[16] Mansour MA, El-Hakiem MA, El-Kabeir SM. Heat and mass transfer in magneto hydrodynamic flow of a micropolar fluid on a circular cylinder with uniform heat and mass flux, J. Magn. Magn. Mater. 2000; 220: 259–270.

[17] El-Hakiem MA. Viscous dissipation effects on MHD free convection flow over a nonisothermal surface in a micro polar fluid, Int. Commun. Heat Mass Transfer 2000; 27: 581–590.

[18] El-Hakiem MA, Mohammadein AA, El-Kabeir SMM. Joule heating effects on magneto hydrodynamic free convection flow of a micro polar fluid, Int. Commun. Heat Mass Transfer 1999; 26: 219–227.

[19] El-Amin MF. Magnetohydrodynamic free convection and mass transfer flow in micropolar fluid with constant suction, J. Magn. Magn. Mater. 2011; 234: 567–574.

[20] Kim YJ. Unsteady MHD convection flow of polar fluid past a vertical moving porous plate in a porous medium, Int. J. Heat Mass Transfer 2001; 44: 2791–2799.

[21] Rashidi MM, Mohimanian Pour SA, Abbasbandy S. Analytic approximate solutions for heat transfer of a micropolar fluid through a porous medium with radiation, Commun. Nonlinear Sci. Numer. Simul. 2011; 16: 1874–1889.

[22] Shadloo MS, Kimiaeifar A, Bagheri D. Series solution for heat transfer of continues stretching sheet immersed in a micropolar fluid in the existence of radiation, Int. J. Numer. Methods Heat Fluid Flow 2013; 23: 289–304.

[23] Qasim M, Khan I, Shafie S. Heat transfer in a micropolar fluid over a stretching sheet with Newtonian heating, PLoS ONE 2014; 8: e59393.

[24] Pal D, Chatterjee S. Heat and mass transfer in MHD non-Darcian flow of a micropolar fluid over a stretching sheet embedded in a porous media with non-uniform heat source and thermal radiation, Commun. Nonlinear Sci. Numer. Simul. 2010; 15: 1843–1857.

[25] Pal D, Chatterjee S. Effects of radiation on Darcy–Forchheimer convective flow over a stretching sheet in a micropolar fluid with non-uniform heat source/sink, J. Appl. Fluid Mech. 2015; 8: 207–212.

[26] Bataller RC. Viscoelastic fluid flow and heat transfer over a stretching sheet under the effects of a non-uniform heat source, viscous dissipation and thermal radiation, Int. J. Heat Mass Transfer 2007; 50: 3152–3162.

[27] Subhas AM, Mahesha N. Heat transfer in MHD viscoelastic fluid flow over a stretching sheet with variable thermal conductivity, non-uniform heat source and radiation, Appl. Math. Model. 2008; 32: 1965–1983.

[28] Mabood F, Ibrahim SM, Rashidi MM, Shadloo MS, Lorenzini G. Non-uniform heat source/sink and Soret effects on MHD non-Darcian convective flow past a stretching sheet in a micropolar fluid with radiation. Int. J. Heat Mass Transfer 2016;93: 674–682

[29] Rashad AM, Chamkha AJ, El-Kabeir SMM. Effect of chemical reaction on heat and mass transfer by mixed convection flow about a sphere in a saturated porous media, Int. J. Numer Methods Heat Fluid Flow 2011;21: 418–433.

[30] Magyari E, Chamkha AJ. Combined effect of heat generation or absorption and first-order chemical reaction on micropolar fluid flows over a uniformly stretched permeable surface: the full analytical solution, Int. J. Therm. Sci. 2010; 49: 1821–1828.

[31] Damseh RA, Al-Odat MQ, Chamkha AJ, Shannak BA. Combined effect of heat generation or absorption and first-order chemical reaction on micropolar fluid flows over a uniformly stretched permeable surface, Int. J. Therm. Sci. 2009; 48: 1658–1663.

[32] Das K. Effect of chemical reaction and thermal radiation on heat and mass transfer flow of MHD micropolar fluid in a rotating frame of reference, Int. J. Heat Mass Transfer 2011; 54: 3505–3513.

[33] Hayat T, Abbas Z, Ali N. MHD flow and mass transfer of a upper-convected Maxwell fluid past a porous shrinking sheet with chemical reaction species, Phys. Lett. A 2008; 372: 4698–4704.

[34] Bhattacharyya K, Layek GC. Chemically reactive solute distribution in MHD boundary layer flow over a permeable stretching sheet with suction or blowing, Chem. Eng. Commun. 2010; 197: 1527–1540.

[35] Kandasamy R, Muhaimin I, Khamis AB. Thermophoresis and variable viscosity effects on MHD mixed convective heat and mass transfer past a porous wedge in the presence of chemical reaction, Heat Mass Transfer 2009; 45: 703–712.

[36] Afify A. MHD free convective flow and mass transfer over a stretching sheet with chemical reaction, Heat Mass Transfer 2004; 40: 495–500.

[37] Mabood F, Khan WA, Ismail AIM. MHD stagnation point flow and heat transfer impinging on stretching sheet with chemical reaction and transpiration, Chem. Eng. J. 2015; 273: 430–437.

[38] Motsa SS, Dlamini PG, Khumalo M. Spectral relaxation method and spectral quasilinearization method for solving unsteady boundary layer flow problems, Adv. Math. Phys. 2014, Article ID 341964, 12 p.

[39] Andersson HI, Aarseth JB, Dandapat BS. Heat transfer in a liquid film on unsteady stretching surface, Int. J. Heat Mass Transfer 2000; 43(1): 69–74.

[40] Abd El-Aziz M. Mixed convection flow of a miropolar fluid from an unsteady stretching sheet surface with viscous dissipation, J. Egypt. Math. Soc. 2013, 21, 385–394.

[41] Bellman RE, Kalaba RE. Quasilinearization and Nonlinear Boundary-Value Problems, Elsevier, New York, NY, USA, 1965.